PHYSICAL REVIEW B VOLUME 24, NUMBER 10 15 NOVEMBER 1981

Cascading in optical third-harmonic generation by crystalline quartz

Gerald R. Meredith
Webster Research Center, Xerox Corporation, Webster, New York 14580
(Received 27 March 1981)

Cascading, a process whereby lower-order effects combine to contribute to a higher-order nonlinear process, in optical third-harmonic generation (THG) is reported. By using the wedge-fringing method to observe the interference between bound and free waves at the third harmonic, the presence of two bound waves is verified. Theoretical development shows one bound wave to be due to true third-order nonlinearity plus a cascaded contribution involving the bound wave of second-harmonic generation. The other bound wave arises solely due to cascading involving the free wave of second-harmonic generation. Considerations of crystal and wave-vector orientations are presented, and a method of effective fields is used to account for cascading through local fields. α-quartz was studied, allowing verification of the cascading by symmetry as well. A treatment is presented for the THG intensity-altering effect of gases surrounding condensed-phase materials. Finally, the specific observation of interferences among the several waves allows a direct calibration of $X^{(3)}(-3\omega,\omega,\omega,\omega,)$ relative to the product $X^{(2)}(-3\omega,2\omega,\omega)X^{(2)}(-2\omega,\omega,\omega)$ of quartz for the 1.91-μm fundamental wavelength employed here.

I. INTRODUCTION

It is by now well known that lower-order optical nonlinearities contribute in multistep or cascaded fashion to higher-order nonlinear phenomena.[1-5] The basic concept is that nonlinear polarizations produced in low-order processes generate intermediate macroscopic electric fields in addition to those directed upon the sample by the experimenter. These intermediate fields may interact nonlinearly with the purposely impressed fields to generate polarization which contributes to the process under investigation. While phase matching of the process which generates the intermediate wave is not typical, it may be utilized near resonances to study polariton characteristics.[1] More generally when that process is non-phase-matched, both free and bound intermediate waves result.[2] If the higher-order process being observed is phase matched, cascaded interactions involving exclusively the intermediate bound waves will also be phase matched. An appreciation of this resultant contribution to the overall phase-matched process is consequently essential for the extraction of true nonlinear susceptibilities[2] or the prediction of the magnitudes of such phase-matched nonlinear effects. In this article we report the consequences of cascading in the study of a non-phase-matched higher-order process and obtain a calibration of the true higher-order susceptibility in terms of the lower-order susceptibilities which contribute in the cascading.

Non-phase-matching is the situation for the accurate Maker or wedge-fringing techniques of measurement of nonlinear susceptibilities.[6] These methods rely on the interference of the nonlinearly generated bound and free waves for determining coherence lengths and susceptibilities. For this work we employ the wedge-fringing technique which displays these interferences by altering the physical length of the crystal traversed by the beams by a suitable transverse translation of the wedge. A new observation which we consequently make is the addition of a second bound wave in a higher-order process due to the presence of an intermediate *free* wave in the cascading process. This term has been theoretically suppressed in earlier cascading studies where (nearly) phase-matched third-order processes were monitored.[2,3] This is reasonable since at the monitored frequency the non-phase-matched bound wave has a coherence length which is generally much shorter than the crystal length. Many cycles of phase between free and bound waves occur across the crystal. A negligible contribution obtains from this mechanism in relation to that obtaining from the phase-

matched bound wave involving the true higher-order effect plus the cascading with the intermediate bound wave. Under those circumstances the presence of the totally bound cascaded contribution was confirmed only by geometric considerations, that is, by measurement with different vector orientations, in high-symmetry crystals. In the experiments reported here the presence of cascading and the evaluation of relative contributions are made in a single polarization setting. It is suggested that this is important since with low-symmetry crystals one does not have the luxury of additional constraints to deduce the cascaded contributions and may not wish to perform the measurement of all elements of the lower-order susceptibility tensors needed to calculate those contributions.

We chose perhaps the simplest situation in which to observe these phenomena: third-harmonic generation in a noncentrosymmetric crystal. Cascading may be observed in third order of nonlinearity only in macroscopically noncentrosymmetric media since nonvanishing second-order effects are required. By using α-quartz we were also able to confirm the cascading by resorting to symmetry as done in earlier works as a supplement to the direct single polarization setting method. That is, by choosing two crystal orientations and polarization settings for which the true third-order responses are equal by symmetry but the second-order responses are not, the observed difference in total third-order response was used to characterize the cascading. In addition, the cascading which is described by a product of two second-order susceptibilities beats directly against the contribution due to the true third-order susceptibility allowing an accurate calibration of the latter relative to the former. This feature was utilized to calibrate third-order susceptibilities and to deduce bond characteristics of GaAs by the Bloembergen group.[2] We were able in this work to perform this type of calibration with high precision for α-quartz, thus generating a useful standard for future third-harmonic-generation studies in the visible.[7]

In the remainder of this paper we will discuss the detailed theory of macroscopic field cascading in third-harmonic generation with a simplified discussion of the local or microscopic field cascading as an appendix, the role of symmetry in determining the varieties of macroscopic field cascading in α-quartz, the important but previously neglected influence of gases surrounding a sample being studied by non-phase-matched third-order processes, and our experiments and conclusions.

II. THEORY

A. Cascading in third-harmonic generation (THG)

In this section the various electric and nonlinear polarization waves involved in the production of light at frequency 3ω from an intense fundamental wave in a noncentrosymmetric crystal will be described in a scalar formalism. In the plane-wave small-conversion approximation an intense monochromatic electric field with frequency ω and wave vector $k_f^{\omega}\hat{z}$ directed along the z axis,[8]

$$E(r,t)=E^{\omega}(r)+\text{c.c.}\ , \tag{2.1}$$

$$E^{\omega}(r)=E^{\omega}\exp(ik_f^{\omega}z)$$
$$=|E^{\omega}|\exp[i(k_f^{\omega}z-\omega t)]\ , \tag{2.2}$$

directly produces *nonlinear* source polarizations at frequencies 2ω and 3ω through the nonlinear susceptibilities:

$$P^{2\omega}(r)=X^{(2)}(-2\omega,\omega,\omega)(E^{\omega})^2\exp(ik_b^{2\omega}z)\ , \tag{2.3}$$

$$P^{3\omega}(r)=X^{(3)}(-3\omega,\omega,\omega,\omega)(E^{\omega})^3\exp(ik_b^{3\omega}z)\ . \tag{2.4}$$

If there is an interface between optically linear and nonlinear media at $z=0$, some electric fields which arise in the crystal are[9]

$$E^{2\omega}(r)=E_f^{2\omega}\exp(ik_f^{2\omega}z)+E_r^{2\omega}\exp(-ik_r^{2\omega}z)$$
$$+E_b^{2\omega}\exp(ik_b^{2\omega}z)\ , \tag{2.5}$$

$$E^{3\omega}(r)=E_f^{3\omega}\exp(ik_f^{3\omega}z)+E_r^{3\omega}\exp(-ik_r^{3\omega}z)$$
$$+E_b^{3\omega}\exp(ik_b^{3\omega}z)+E_b^{3\omega'}\exp(ik_b^{3\omega'}z)\ . \tag{2.6}$$

The E_f, E_r, and E_b terms are forward-travelling free waves, reflected free waves and forward bound waves. The E_r may be removed by applying boundary conditions at the interface.

Cascading requires the inclusion of the additional source polarization at 3ω:

$$P^{3\omega}(r)'=2X^{(2)}(-3\omega,2\omega,\omega)$$
$$\times[E^{2\omega}(r)+(L^{2\omega}/f^{2\omega})P^{2\omega}(r)]E^{\omega}(r)\ . \tag{2.7}$$

The second term in the bracket is the result of cascading through the local field. As discussed in Appendix A, its effect can be subsumed in an effective bound wave $(E_b^{2\omega})_{\text{eff}}$. Ignoring contributions of reflected waves to nonlinearities and using primed-unprimed frequency notation shorthand to allow suppression of cumbersome arguments,

$$P^{3\omega}(r)' = 2X^{(2)\prime} E_f^{2\omega} E^{\omega} \exp(ik_b^{3\omega\prime} z) + 2X^{(2)\prime} (E_b^{2\omega})_{\text{eff}} E^{\omega} \exp(ik_b^{3\omega} z) . \quad (2.8)$$

For colinear geometry the wave vectors are directly related to refractive indices and angular frequencies:

$$k_f^{q\omega} = (q\omega/c) n_{q\omega} ,$$
$$k_b^{2\omega} = 2k_f^{\omega} ,$$
$$k_b^{3\omega} = 3k_f^{\omega} , \quad (2.9)$$
$$k_b^{3\omega\prime} = k_f^{2\omega} + k_f^{\omega} = (3\omega/c) n_e .$$

And for definiteness, assuming only transverse waves,

$$E_b^{2\omega} = -[16\pi l_c^{2\omega}/\lambda(n_{\omega} + n_{2\omega})](E^{\omega})^2 X^{(2)} \quad (2.10)$$

$$E_b^{3\omega} = -[24\pi l_c^{3\omega}/\lambda(n_{\omega} + n_{3\omega})](E^{\omega})^3 \times \{X^{(3)} - [32\pi l_c^{2\omega}/\lambda(n_{\omega} + n_{2\omega})] \times X^{(2)} X^{(2)\prime} [(E_b^{2\omega})_{\text{eff}}/E_b^{2\omega}]\} \quad (2.11)$$

$$E_b^{3\omega\prime} = -[48\pi l_c^{3\omega\prime}/\lambda(n_e + n_{3\omega})] E_f^{2\omega} E^{\omega} X^{(2)\prime} . \quad (2.12)$$

Anticipating that for all frequencies of interest $k_b < k_f$, we have defined the coherence lengths to be positive ($|k_b - k_f| l_c = \pi$). $E_f^{2\omega}$ and also $E_b^{3\omega\prime}$ are determined by the optical properties of the linear medium as well as the nonlinear medium. For normal incidence to an interface with vacuum

$$E_f^{2\omega} = -[(1+n_{\omega})/(1+n_{2\omega})] E_b^{2\omega} . \quad (2.13)$$

The substitution to obtain $E_b^{3\omega\prime}$ may be easily made:

$$E_b^{3\omega\prime} = -[24\pi l_c^{3\omega\prime}/\lambda(n_e + n_{3\omega})][(1+n_{\omega})/(1+n_{2\omega})][32\pi l_c^{2\omega}/\lambda(n_{\omega} + n_{2\omega})](E^{\omega})^3 X^{(2)} X^{(2)\prime} . \quad (2.14)$$

Then for another interface to vacuum at $z = l$, the 3ω field at l^+ is

$$E^{3\omega}(l^+) = \{[B' \exp(i\pi l/l_c^{3\omega}) - B] E_b^{3\omega} + [C' \exp(i\pi l/l_c^{3\omega\prime}) - C] E_b^{3\omega\prime}\} \exp(ik_f^{3\omega} l) , \quad (2.15)$$

where

$$B = 2n_{3\omega}(1+n_{\omega})/(1+n_{3\omega})^2 ,$$
$$B' = (n_{\omega} + n_{3\omega})/(1+n_{3\omega}) ,$$
$$C = 2n_{3\omega}(1+n_e)/(1+n_{3\omega})^2 , \quad (2.16)$$
$$C' = (n_e + n_{3\omega})/(1+n_{3\omega}) .$$

The intensity of light at 3ω is

$$I^{3\omega} = (c/2\pi) |E^{3\omega}(l^+)|^2 . \quad (2.17)$$

Although there are only two modulating terms in the field, Eq. (2.15), there will be three modulating terms in the intensity. The additional term will vary with the difference of spatial frequencies of the two bound 3ω waves.[10] Further contributions would result and must be added to Eq. (2.17) if cascading could simultaneously occur through a second transverse intermediate or a longitudinal intermediate second harmonic (see below).

We have retained the precise form of the coefficients rather than make the approximations $B \simeq B' \simeq C \simeq C'$ which are good to better than 1% in the experiments here, but which may become the limiting error in more dispersive cases. Some care was taken in defining the notation since an explicit and consistent formalism is especially needed when combining more than one order of nonlinearity. Additionally, the notation was chosen to emphasize observables of the wedge-type experiment.

Two points should be emphasized about the contributions inherent in Eq. (2.17). First, $E_b^{3\omega}$ of Eq. (2.11) appears as a normal bound wave resulting from the third-order response of the material to the fundamental wave but with the modification that the usual $X^{(3)}$ factor is altered by a term involving the product of two second-order susceptibilities. This alteration depends on the characteristics of the crystalline material under study as well as the frequency ω chosen and may vary from being negligible to dominant in comparison to $X^{(3)}$. Second, the appearance of the second bound wave $E_b^{3\omega\prime}$, which results in three spatially modulated contributions to $I^{3\omega}$ rather than the single component of the usual Maker or wedge experiments, is correlated to the occurrence of the just mentioned alteration of $X^{(3)}$. Barring drastically different $l_c^{3\omega}$ and $l_c^{3\omega\prime}$ the failure to observe complex fringing due to the presence of $E_b^{3\omega\prime}$ would assure that the $X^{(3)}$ term of $E_b^{3\omega}$ is minimally altered by

transverse cascading and (for negligible longitudinal cascading) a true susceptibility may be simply extracted from the fringe height and period. Conversely, the observation of complex fringing requires an analysis of the sort used below to separate the true $X^{(3)}$ from the additional cascading contribution.

B. Anisotropies in α-quartz

In this section specific limitations of the results of the preceding section imposed by details of the α-quartz crystal structure will be discussed. The nonzero matrix elements of $X^{(2)}(-2\omega,\omega,\omega)$, $X^{(2)}(-3\omega,2\omega,\omega)$, and $X^{(3)}(-3\omega,\omega,\omega,\omega)$ in α-quartz are listed in Table I where symmetry conditions of the $P3_221$ (right-handed enantiomorph) space group have been applied.[11] The importance of such tables cannot be overly stressed since the equations so cavalierly written in scalar notation above are, in fact, tensor equations. In addition, for optically nonisotropic crystals the orientation of E and P relative to the normal crystal vibration directions as functions of wave-vector direction must be properly treated. We avoid the complexity of nonparallelness of E, P, and D by choosing principal polarizations and allow the neglect of optical activity by avoiding optic axis propagation. In quartz principal directions are the z axis or the x-y plane. Under these restraints the use of Table I to check for symmetry-allowed cascading is merely an exercise in picking all nonzero $X^{(2)}_{inj}(-3\omega,2\omega,\omega)X^{(2)}_{nkl}(-2\omega,\omega,\omega)$ for each $X^{(3)}_{iikl}$.

Consulting Table I it is clear that $X^{(3)}_{zzzz}$ is the only element for which macroscopic cascading never occurs. For $X^{(3)}_{xxxx}$ macroscopic cascading occurs only through $X^{(2)}_{xxx}X^{(2)}_{xxx}$, which is the simplest case since the $E^{2\omega}_x$ intermediate field is transverse and no other macroscopic cascades are possible. A measurement of $X^{(3)}_{yyyy}$ is nearly equivalent with $\vec{k}||\hat{z}$, but in this configuration optical activity is a complicating factor which we wish to avoid here. A different effect arises if one takes $\vec{k}||\hat{x}$; longitudinal E_x obtains. For this situation, temporarily resorting to tensor notation, consideration of the wave equation (remembering that $P^{2\omega}$ is only the nonlinear source polarization)

$$[(\vec{\nabla}\times\vec{\nabla}\times)-(4\omega^2/c^2)\vec{\epsilon}_{2\omega}]\cdot\vec{E}^{2\omega}_b(r) = (16\pi\omega^2/c^2)\vec{P}^{2\omega}(r) \quad (2.18)$$

requires

$$\vec{E}^{2\omega}_b(r)=-[4\pi/(\epsilon_{2\omega})_{xx}]\vec{P}^{2\omega}(r)\ . \quad (2.19)$$

Since $\vec{D}^{2\omega}=\vec{\epsilon}_{2\omega}\cdot\vec{E}^{2\omega}_b(r)+4\pi\vec{P}^{2\omega}(r)=0$, the boundary conditions are automatically fulfilled so that no internal free wave $E^{2\omega}_f$, is generated. The final result of the preceding section describing the resulting third-harmonic fields and intensities applies with

$$E^{3\omega\prime}_b=0\ , \quad (2.20)$$

TABLE I. Nonzero susceptibility matrix elements of α-quartz.

$X^{(2)}=X^{(2)}_{nkl}(-2\omega,\omega,\omega)$	$X^{(2)\prime}=X^{(2)}_{inj}(-3\omega,2\omega,\omega)$	$X^{(3)}=X^{(3)}_{ijkl}(-3\omega,\omega,\omega,\omega)$
$xxx=-R\{2y\rightarrow 2x\}$[a]	$xxx=-R\{2y\rightarrow 2x\}$	$zzzz$
$xyz=-yxz$	$xyz=-yxz$	$xxxx=yyyy$
$=xzy$	$xzy=-yzx$	$=3R\{2y\rightarrow 2x\}$
$=-yzx$		
	$zxy=-zyx$	$xxzz=xzxz=xzzx$
		$=R\{2y\rightarrow 2x\}$
		$zzxx=zxzx=zxxz$
		$=R\{2y\rightarrow 2x\}$
		$yyyz=yyzy=yzyy$
		$=-R\{2x\rightarrow 2y\}$
		$zyyy=-R\{2x\rightarrow 2y\}$

[a] $R\{2y\rightarrow 2x\}$ symbolizes any member of the set of elements obtained by replacing any two x polarization indices with two y indices.

$$E_b^{3\omega} = -[24\pi l_c^{3\omega}/\lambda(n_\omega + n_{3\omega})](E^\omega)^3 \times \{X^{(3)} - (8\pi/\epsilon_{2\omega})X^{(2)}X^{(2)\prime}\,[(E_b^{2\omega})_{\text{eff}}/E_b^{2\omega}]\}\ . \tag{2.21}$$

The cascaded term contained in Eq. (2.21) has no directly observable consequences, but merely causes a reduction of the net THG (assuming real positive susceptibilities). A quick estimate using Lorentz local fields shows the susceptibility reduction of $X^{(3)}_{yyyy}$ by longitudinal cascading to be only $\sim 1\%$ of the corresponding reduction of $X^{(3)}_{xxxx}$ in the transverse case for the particular experiments reported here. The situation for other polarization settings can be similarly handled and quickly becomes algebraically complicated. A simplification arises if Kleinmann symmetry is applied. The near validity of this approximation implies $|X^{(2),(2)\prime}_{P\{xyz\}}| << |X^{(2),(2)\prime}_{xxx}|$, where $P\{xyz\}$ signifies all permutations of the three indices.

One can see from the cases explicitly examined above (e.g., *xxxx* polarization setting versus *yyyy* setting with $\vec{k}||\hat{x}$) that although each of the individual orders of *true* susceptibility strictly obeys the symmetry requirements of the crystal (e.g., $X^{(3)}_{xxxx} = X^{(3)}_{yyyy}$), when an intense plane-wave electric field is impressed upon the crystal, the responses which are third order in the field would not be described overall by an effective third-order susceptibility with the full crystal symmetry [e.g., $(E_b^{3\omega})_x \neq (E_b^{3\omega})_y$]. The inclusion of the nonlocal, and therefore symmetry reducing, cascading is responsible due to the directed wave nature. These symmetry characteristics are in contradiction to the earlier conclusion of Flytzanis[4] for the real cases $k \neq 0$. In conjunction with the comments at the end of the last section the magnitude of this deviation depends on the relations of the linear, second-order, and third-order susceptibilities of the specific crystal at the chosen fundamental frequency and may be drastic if cascading dominates the direct third-order response.

C. Effects of gases in third-harmonic generation

Ward and New[12] have presented a thorough treatment of third-harmonic generation with special attention given to harmonic generation in infinite media with focused Gaussian beams. Their conceptually simple presentation of results via vibration diagrams will be followed here to display effects pertinent to the generation of third harmonic by a thin solid slab surrounded by a gaseous atmosphere. We refer to their work for details of the vibration diagram method but recall here the simple interpretative point that the magnitude of the electric field is proportional to the distance in the vibration plane between the point on a vibration diagram corresponding to the observation point and its origin point $(-\infty)$. Some electric vectors are symbolized for illustrative purposes according to the Ward and New method with a double arrow in our diagrams. Also recall that $\Delta k = k_b - k_f$ and is negative for normally dispersive materials.

Figure 1(a) displays the situation of infinite media non-phase-matched harmonic generation (single bound wave) in a plane-wave approximation with $\Delta k < 0$ and real. The $\sin^2(\pi l/l_c)$ dependence is obvious. The magnitude of the field increases with the radius of the circle which increases as $|X/\Delta k|$. Figure 1(b) depicts THG in an infinite medium with a focused Gaussian beam for $\Delta k = 0$. ξ is a coordinate normalized for focusing strength and centered at the minimum waist [$\xi = 2(z-f)/b$

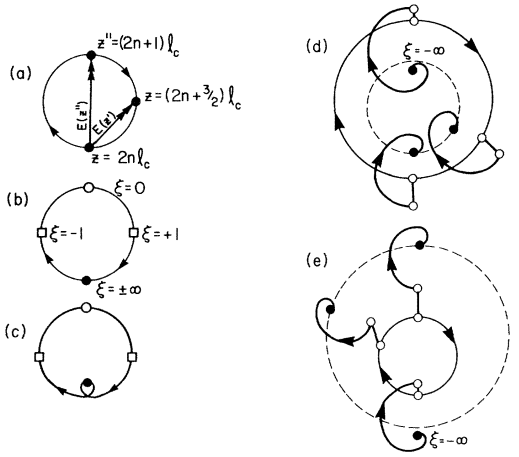

FIG. 1. Vibration diagrams after Ward and New (Ref. 12) to describe THG with focused beams and with thin solids in gaseous environment. (a) Simple non-phase-matched harmonic generation with plane waves. (b) THG in infinite medium from focused Gaussian fundamental with $\Delta k = 0$. (c) Similar to (b) with $b\Delta k \simeq 0.3$. (d) THG from a very thin solid with shorter coherence length placed at focal position of the fundamental Gaussian and surrounded by an infinite nonlinear dielectric with $\Delta k \neq 0$; $X^{(3)}/\Delta k$ same sign and $\Delta k < 0$ for both media. Two cases corresponding to different amounts of retardation in the crystal are presented. The set of final $\xi = +\infty$ points forms a circle represented with dashes. (e) Similar to (d) with $X^{(3)}/\Delta k$ changing sign between media. See text for a fuller discussion.

where f is the value of z at focus and b the confocal parameter]. Figure 1(c) depicts the same case but for $b\Delta k \simeq -0.3$. The amount of curvature can increase substantially resulting in tightly spiraled figures for $|b\Delta k| >> 1$. An important point is that the net third harmonic is always zero for $\Delta k \leq 0$ even though finite values of $E^{3\omega}$ exist between $\xi = -\infty$ and $+\infty$.

The utility we wish to make of these diagrams is to portray the influence of the gas surrounding a crystal being studied via THG. For this end it is merely a matter of splicing together portions of vibration diagrams such as 1(a) and 1(c). At each interface in the experiment a splice is made of the appropriate sections and an offset along the corresponding direction of $E^{3\omega}$ must be made to correct for dielectric transmission factors. One should also include the effect of reduced fundamental intensity but possibly increased field strength on passing through each interface for determining the nonlinear driving elements. To approximate the physical situation of a thin crystal in a slowly focused beam the width of the crystal will be ignored in the gas portions of the diagrams and splices will occur at $\xi = 0$. Figure 1(d) shows this situation for gas and crystal susceptibilities having identical signs. The set of possible $\xi = +\infty$ points create a (dashed) circle[13] which does not, but nearly does, cross the $\xi = -\infty$ point. Figure 1(e) is the case where the susceptibilities have opposite sign. For this situation at the interfaces the infinitesimal vibration element reverses direction but $\Delta k < 0$ preserves the clockwise rotation of the curve. In both cases $A + \sin^2[(\pi l/l_c) + \varphi]$ intensity behavior is predicted, but the resultant THG magnitude is not characteristic of the crystal alone. The additional contribution depends on b, Δk, and $X^{(3)}$ of the gas. For this reason experiments of the nature described here which are intended for calibration must be done in vacuum.

III. EXPERIMENTAL

The details of the apparatus used to generate and detect the third harmonic will be presented elsewhere.[14] Briefly, the singly Stokes shifted light at 1.9μm resulting from passage of a Q-switched Nd^{3+} yttrium aluminum garnet (YAG) laser 1.06-μm beam through a pressurized hydrogen-gas Raman cell was filtered with glass filters and focused over a distance of 95 cm. A 10% single surface reflection was split off prior to the focal region and used in a reference arm where a red Corning glass filter produced sufficient third harmonic for pulse-by-pulse normalization. In the sample arm a polarization rotator before the sample and glan prism polarizer after were used to set polarization conditions. No polarizer was needed with the Raman source since a high degree of polarization was carried over from the polarized 1.06-μm laser. In both arms glass filters to attenuate the fundamental followed by 20-cm focal length monochromators isolated the harmonic. The monochromators were oriented to reduce polarization dependence of the throughput; tests showed the intensity differential between the two polarizer positions to be less than 1%. Photomultipliers were used for detection except when silicon photodiodes in homemade operational amplifier circuits were substituted to detect the second harmonic. Computer-controlled gated integration, digitization, and analysis followed.

The two degree wedged crystals of quartz were placed in the center of a 72-cm vacuum-pressure optical cell, which was positioned with the center at the beam waist on a transversely mounted translation stage. The stage was driven via a stepper motor under computer control. The change in thickness of crystal traversed by the beam was determined by the simple relation $\delta l = 2x \tan(\alpha/2)$, where α is the wedge angle and x the transverse displacement. The large wedge angle of the available crystals and the large beam waist at focus caused convolution of the resulting fringing signals. Empirical correction was applied as described in Appendix B.

The 1.91-μm beam was definitely not Gaussian. The 1.06-μm beam had a depleted middle and the nonlinear Raman conversion amplified the effect. Despite this no detectable THG was seen from the apparatus, even with the cell evacuated or pressurized to two atmospheres, unless a sample (quartz, fused silica, glass, etc.) was placed within the focal region. This shows the validity of the focusing considerations even for non-Gaussian profiles.

IV. RESULTS AND DISCUSSION

In Fig. 2(a) the THG wedge fringes from a two degree quartz y-cut wedge in vacuum with $xxxx$ polarization selection are presented. The least-squares best fit of Eq. (2.17) to the data also appears. The offset of the minima of fringes from zero is partially a consequence of the functional

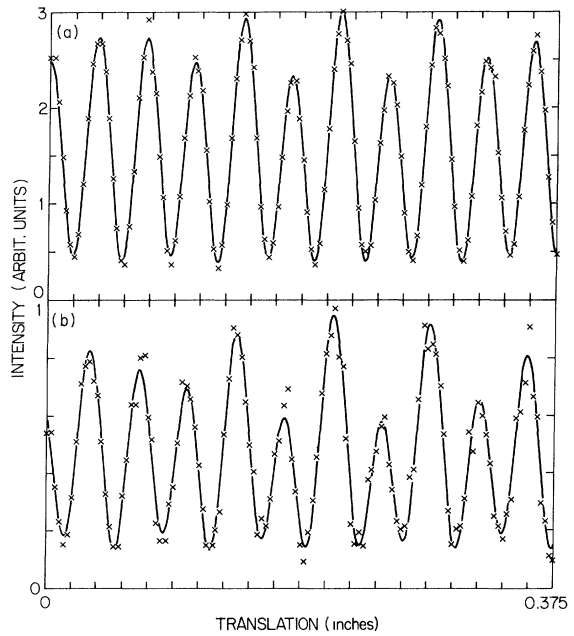

FIG. 2. Third-harmonic wedge fringes from a y-cut α-quartz crystal. Fundamental and harmonic are polarized parallel to x. (a) Crystal in vacuum. (b) Crystal in one atmosphere of nitrogen. The relative scales are accurate.

form and partially of convolution of fringes due to the finite size of the beam waist. Figure 2(b) presents similar results for the same wedge in one atmosphere of nitrogen gas. To emphasize the importance of the gas contribution to the total THG intensity as described in the theoretical section, the relative scales should be noted. We have observed this drastic alteration of intensity with surrounding gas pressure in other polarization conditions and for wedges of fused silica and BK-7 glass. One can rationalize the magnitude of this effect in the following manner. THG electric field strengths in non-phase-matched configuration scale with $X^{(3)}/\Delta k$. However, since both numerator and denominator scale roughly with density, gases may make contributions comparable to those of condensed phases. In fact Ward and New[12] noted that for this reason THG signals from gases approach a high-pressure limit. Furthermore, although $X^{(3)}$ for the gases that they studied varied over several orders of magnitude, this ratio was much more restricted. The implication of the latter is that even though a gas such as helium has a negligibly small nonlinear susceptibility, it cannot be used to replace the air surrounding the crystal in these types of experiments without generating substantial error since it also has small linear susceptibility. In light of Figs. 1(d) and 1(e) the implication of our reduced signals at high gaseous pressure is that $X^{(3)}$ of nitrogen, air, helium, and the solids studied here have the same sign: positive, as is confirmed below through considerations of cascading.

The $E^{3\omega}$ due to THG occuring in the nitrogen up to the interface propagates through the crystal as a free wave. Its phase relation to $E_b^{3\omega}$ on entering nitrogen again at the second interface behaves identically to the phase relation of $E_f^{3\omega}$ and $E_b^{3\omega}$ of quartz just across the interfaces. Therefore, the nature of the gas contribution is to decrease the effectiveness of $E_b^{3\omega}$ in generating fringes while leaving $E_b^{3\omega'}$ unaltered. In fact in Figs. 1(a) and 1(b) the ratio of values of $E_b^{3\omega'}$ from the fits is 1.019, the deviation from 1 being an indication of the overall stability and reproducibility of our fringes and fittings, while the ratio of values of $E_b^{3\omega}$ is 0.491. This is apparent in the markedly different amplitude modulation of the high-frequency fringes whose effect is due to the nearly factor of 2 ratio between $l^{3\omega}$ and $l^{3\omega'}$. It was thought to be an interesting experiment to use the specificity of gaseous interference to totally cancel the contribution of $E_b^{3\omega}$ to the THG intensity and observe only the free-wave intermediate cascading fringes. Attempts to find the appropriate pressure of nitrogen were unsuccessful apparently because the high-pressure limit of the nitrogen THG electric field in the focal region of our particular experimental apparatus is smaller than $E_b^{3\omega}$.

Several aspects of the fitted fringe data warrant attention. Associated with the comment following Eq. (2.17) there is a relationship among the coherence lengths occuring therein:

$$(l_c^{2\omega})^{-1}=(l_c^{3\omega})^{-1}-(l_c^{3\omega'})^{-1}\,. \tag{4.1}$$

Using the values 15.89 and 28.45 μm derived from the fits for $l_c^{3\omega}$ and $l_c^{3\omega'}$, respectively, $l_c^{2\omega}=36.01$ μm is predicted. Second-harmonic-generation (SHG) wedge fringes were observed from the same crystal and the least-squares fit returned a value of 36.10 μm. These values are a few percent higher than would be calculated from refractive indices,[15] perhaps indicating that the wedge angle is slightly less than the nominal 2° specified by the manufacturer or that nonlinear refractive index changes are occurring. The latter, however, seems unlikely with simple considerations of $n^{(2)}$. Nevertheless, the quality of the curve fitting and the agreement between independent experiments confirms that cascading is the primary additional process complicating the THG fringes of

Fig. 1.

To test the accuracy of the derived parameters and the formalism, the anisotropy of the THG fringing was studied and found to be consistent with the discussion of Sec. II B. High-quality purely sinusoidal fringes were detected from an x-cut quartz 2° wedge with $yyyy$ polarization selection confirming $E_b^{3\omega\prime}=0$ for this case. The same held for $zzzz$ polarization with either of the two wedges. By normalizing with the $zzzz$ signals the ratio of $(E_b^{3\omega})_x$, a transverse case, to $(E_b^{3\omega})_y$, a longitudinal case, was determined to be 0.952 ± 0.031. From the fit parameters it was established that for transverse cascading the second term in Eq. (2.11), the bound-wave cascading term, is 7.4% of the first. By using appropriate numerical values with the assumption of a Lorentz local field, the longitudinally cascaded term in Eq. (2.21) is seen to be a factor of 110 smaller than in Eq. (2.11), thus showing cascading and the details of the local-field model to be insignificant for the longitudinal case. It is important to note that this conclusion could not have been reached in the absence of the transverse study or prior knowledge of $X^{(2)}$, $X^{(2)\prime}$, and $\epsilon_{2\omega}$; clearly, observation of good sinusoidal fringes does not imply measurement of $X^{(3)}$ without a cascaded alteration. Then the agreement between the cascading diminution of $(E_b^{3\omega})_x$ as described in Eq. (2.11) and the difference of $(E_b^{3\omega})_x$ from $(E_b^{3\omega})_y$ as described in Eq. (2.21) is good considering the experimental difficulties involved in the accurate comparisons of sequential fringing patterns on two different crystals and further confirms the interpretation.

One of the objectives of this work was to generate a reliable standard for THG studies of molecular hyperpolarizabilities being conducted in our laboratory. The cascading observed here has provided a direct link to the highly studied second-order susceptibilities. To obtain a calibration the following literature data was considered. Choy and Byer recently performed accurate absolute calibration of d_{31} in $LiIO_3$ and $LiNbO_3$.[16] Using Miller Δ formalism they generated recommended d values for several materials at several wavelengths. Combining their $d_{31}(LiIO_3)_{\lambda=1.06\mu m}=7.11\times10^{-12}$ m/V and Jerphagnon's[17] $[d_{31}\ (LiIO_3)/d_{11}(SiO_2)]_{\lambda=1.06\mu m}=15.5\pm0.8$ yields $d_{11}(SiO_2)_{\lambda=1.06\mu m}=1.095\times10^{-9}$ esu. Also, combining their $d_{36}(KDP)_{\lambda=1.06\mu m}=0.630\times10^{-12}$ m/V with Jerphagnon and Kurtz's[18] $[d_{11}(SiO_2)/d_{36}\ (KDP)]_{\lambda=1.06\mu m}=0.77\pm0.04$ yields $d_{11}(SiO_2)_{\lambda=1.06\mu m}=1.158\times10^{-9}$ esu. The average value will be adopted here, which results in $X^{(2)}_{xxx}(-2\omega,\omega,\omega)=2.25\times10^{-9}$ esu at 1.06 μm. To account for dispersion we also apply the Miller Δ formalism with published refractive index data[15] to obtain $X^{(2)}_{xxx}(-2\omega,\omega,\omega)=2.08\times10^{-9}$ esu for $\lambda=1.91\,\mu$m and, assuming no additional contributions in the nonlinearity mechanism for two applied frequencies (similar to the occurence of antisymmetric components in two-photon transition tensors), $X^{(2)}_{xxx}(-3\omega,2\omega,\omega)=2.18\times10^{-9}$ esu for $\omega=2\pi c/(1.91\,\mu m)$.

Before the magnitude of $X^{(3)}$ can be determined from the adopted values of second-order susceptibilities, the effect of the local-field cascading must be evaluated. Using a Lorentz field, $L=4\pi/3$ and $f=(\epsilon+2)/3$, in Eqs. (A11) and (A12), one calculates that the corrections to convert macroscopic to effective electric fields are -0.94% and -54.1% for the transverse and longitudinal fields in our experiments. The resulting value of $X^{(3)}/X^{(2)}X^{(2)\prime}$ is $(+8.4\pm0.3)\times10^3$. Consequently, $X^{(3)}_{xxxx}(-3\omega,\omega,\omega,\omega)_{\lambda=1.91\mu m}=(+3.81\pm0.15)\times10^{-14}$ esu not including errors in $X^{(2)}$. The sign is unambiguously determined by the fit and is consistent with the reduction of signals when gases surround the crystal if one recalls that positive signs are attributed to their susceptibilities.[12] We have used parameters from the fit of Fig. 2(a) for the analysis since in this case the determination of the ratio of $E_b^{3\omega}$ to $E_b^{3\omega\prime}$ allows a precise determination whereas the sequential polarization setting method used to test these parameters and the anisotropy would produce error limits larger than $\pm50\%$. We see that the details of the local-field model are inconsequential for this analysis as is shown by the fact that the Lorentz model causes only a 1% alteration of the cascaded term of Eq. (2.11) which is only 7% of the direct term.

Our value of $X^{(3)}$ compares favorably with the value determined by Hermann by THG.[19] However, in his work the calibration was made by comparing THG from one crystal with the wave mixing of light of frequencies ω and 2ω where the 2ω light was produced in a separate quartz crystal, an experiment which might be called intercrystal cascading. No observation of the intracrystal effect was made since he apparently only observed one period of the THG Maker fringing. Referring to our Fig. 2 one sees that a good fringe might result, but the amplitude most likely would be incorrect since there is variation from fringe to fringe. Also, no mention is made of the more important effect of the air on his experiment. Therefore, it is evidently

a fortuitous accumulation of errors which brought his value so close to ours. He reports 2.96×10^{-14} esu, which we adjust to 2.54×10^{-14} esu using the above values for $X^{(2),(2)'}$.

A second calibration of the third-order susceptibility of quartz exists. This is the work of Maker and Terhune[20] in which they performed a wave mixing experiment. They used a ruby laser and a stimulated Raman beam generated in benzene (a_{1g}: 992 cm^{-1}) to calibrate $X^{(3)}(-\omega_3,\omega_1,\omega_1,-\omega_2)$ relative to the Raman cross section of benzene. Despite the fact that this quantity is really a separate entity with different contributions from vibrational and electronic motions than the THG susceptibility,[21] their value, $X^{(3)}_{xxxx}(-\omega_3,\omega_1,\omega_1,-\omega_2)=4c_{1111}=4.0\times10^{-14}$ esu, agrees very well with ours. It may be unwise to draw conclusions about the relative importance of these contributions based on their early work. Also, we note the work of Yajima,[22] who concluded that little dispersion of $X^{(3)}$ was introduced in similar wave mixing experiments due to vibrational motion. However, this early work includes sizable error bars which would encompass the deviations above. In fact, he concluded that cascading of the type observed here is unimportant. Since both of the studies cited used colinear focused ω_1 and ω_2 beams and the processes were non-phase-matched, the accuracy of the results are suspect due to air contributions to the overall generation just as for THG. However, coherence lengths for this wave mixing may be many tens of centimeters in gases so the effect would depend on the details of focusing.

Another determination of the third-order nonlinear susceptibility has been made in the conventional electronics frequency region by Gagnepain and Besson.[23] Using $(3\times10^5)(3\times10^4)^n\epsilon^{(n)}(\text{MKS})=X^{(n)}(\text{esu})$ to convert the nth order nonlinear dielectric constant reported by Gagnepain and Besson in MKS units to the nth order nonlinear susceptibility in esu units, some of their results are $X^{(2)}_{111}=6.5\times10^{-8}$ esu, $X^{(3)}_{1111}<6.5\times10^{-12}$ esu, and $X^{(3)}_{3333}=1.2\times10^{-5}$ esu. Care was taken to exclude piezoelectric and electrostrictive effects. Even so it is clear that nuclear motions dominate the low-frequency nonlinear polarization.

Finally, we note that Levine has successfully applied Phillip's bond-charge concepts to calculate some second- and third-order susceptibilities.[24,25] Considering the atomic size difference in SiO_2 and the mechanism described in Ref. 25 involving this difference which produces additional contribution to $X^{(2)}$, it would be interesting to see the ability of the model to fit the linear, quadratic, and cubic electronic susceptibilities which are now known with a high degree of accuracy.

V. CONCLUSION

Cascading through the intermediate bound and free second-harmonic waves has been observed in the non-phase-matched third-harmonic generation by α-quartz. The intermediate free-wave cascading was observed directly since it creates a nonlinear polarization wave at the third-harmonic frequency which has a wave vector different than that describing the direct polarization. The latter is due to true third-harmonic nonlinearity but in addition has a contribution from the cascading involving the bound second-harmonic wave. The interference of both 3ω bound waves resulting from these polarization waves with the free harmonic wave was observed in a wedge-fringe experiment. When proper treatment of the atmospheric interference, which is a major effect, was realized, a calibration of the third-order susceptibility relative to the well-studied second-order susceptibilities was performed. Also, the presence of the cascading term involving the bound second-harmonic wave was confirmed by use of the symmetry requirements of the space group on the various susceptibility tensors. The problem of cascading through the local fields was seen to be minor when approximated with Lorentz fields.

APPENDIX A

In this appendix we wish to give a simple accounting of local and macroscopic fields which results in the necessity to explicitly apply local-field cascading to the macroscopic field equations. Rigorous treatment has been given by Flytzanis[5] and by Bedeaux and Bloembergen.[26] However, the simpler notation of Ducuing[27] will be used for this problem. This treatment presents the basic physics but removes the complicated anisotropies covered by the tensorial treatment with its concomitant non-Abelian algebra.

The microscopic field $(E_\omega)_m$ acting on the electrons of the material differs from the macroscopic field E_ω due to the polarization field:

$$(E_\omega)_m=E_\omega+L_\omega P_\omega=f_\omega E_\omega\ , \tag{A1}$$

where L_ω is influenced by electron localization and theoretically by cavity shapes or dipole summations. Since P_ω is expressed in both microscopic,

$$P_\omega=(X_\omega^{(1)})_m(E_\omega)_m \ , \tag{A2}$$

and macroscopic terms,

$$P_\omega=X_\omega^{(1)}E_\omega \ , \tag{A3}$$

the relation between $(X_\omega^{(1)})_m$ and $X_\omega^{(1)}$ is closed.

Consideration of nonlinearities up to third order result in harmonics $q\omega$, $q=0,1,2,3$. Formally, one writes the *total* polarization density for the macroscopic case

$$P_{q\omega}=X_{q\omega}^{(1)}E_{q\omega}+(P_{\rm NLS})_{q\omega} \ , \tag{A4}$$

and for the microscopic case

$$P_{q\omega}=(X_{q\omega}^{(1)})_m(E_{q\omega})_m+(P_{\rm NL})_{q\omega} \ . \tag{A5}$$

$(P_{\rm NLS})_{q\omega}$ is the macroscopic nonlinear polarization to be used in Maxwell's equations. It is not the simple summation of local nonlinear polarization $(P_{\rm NL})_{q\omega}$, resulting from local fields interacting nonlinearly through the microscopic susceptibilities (hyperpolarisabilities) unless $L=0$. This situation arises due to the local-field contributions from $(P_{\rm NLS})$. One expects

$$(E_{q\omega})_m=E_{q\omega}+L_{q\omega}P_{q\omega} \ , \tag{A6a}$$

which requires

$$(E_{q\omega})_m=f_{q\omega}[E_{q\omega}+(L_{q\omega}/f_{q\omega})(P_{\rm NLS})_{q\omega}] \tag{A6b}$$

on retaining the definition of $f_{q\omega}$ in linear terms from (A1). Using (A6a) in (A5),

$$P_{q\omega}=f_{q\omega}[(X_{q\omega}^{(1)})_mE_{q\omega}+(P_{\rm NL})_{q\omega}] \ , \tag{A7}$$

and utilizing the formal condition (A4), we have

$$(P_{\rm NLS})_{q\omega}=P_{q\omega}-X_{q\omega}^{(1)}E_{q\omega}=f_{q\omega}(P_{\rm NL})_{q\omega} \ . \tag{A8}$$

This is the familiar result that bulk susceptibilities are amplified by an extra local-field factor caused by the *linear* local response to the additional *nonlinearly* generated local field $L_{q\omega}(P_{\rm NLS})_{q\omega}$, of (A6b). Examples are, for SHG and THG,

$$X_{2\omega}^{(2)}=f_{2\omega}(X_{2\omega}^{(2)})_mf_\omega f_\omega \ , \tag{A9}$$

$$X_{3\omega}^{(3)}=f_{3\omega}(X_{3\omega}^{(3)})_mf_\omega f_\omega f_\omega \ . \tag{A10}$$

The difficulty which arises is that the *nonlinear* local responses involving this additional local field have not been included. Practically, one might choose to avoid the complicated formulas of Flytzanis, which produce effective susceptibilities incorporating this local-field cascading, and recognize the bracketed factor of (A6b) as the effective field $(E_{q\omega})_{\rm eff}$ to be applied (self-consistently) when deriving the $P_{\rm NLS}$ from macroscopic fields. We adopt this viewpoint. Only when $E_{q\omega}$ is not generated by a phase-matched interaction and is not an applied field will appreciable error result from its neglect. This is the case for cascading of the type we observe in THG of quartz. The two cases of interest for cascading in THG, transverse and longitudinal $(P_{\rm NLS})_{2\omega}$, are treated here by inclusion in the bound second-harmonic wave.

Transverse:

$$(E_b^{2\omega})_{\rm eff}=[1-(L_{2\omega}/f_{2\omega})(\epsilon_{2\omega}-\epsilon_\omega)/4\pi]E_b^{2\omega} \ . \tag{A11}$$

Longitudinal:

$$(E_b^{2\omega})_{\rm eff}=[1-(L_{2\omega}/f_{2\omega})\epsilon_{2\omega}/4\pi]E_b^{2\omega} \ . \tag{A12}$$

We emphasize that the value of $E_b^{2\omega}$ is not changed. $(E_b^{2\omega})_{\rm eff}$ is only applied for the generation of $P^{3\omega}$.

APPENDIX B

The problem of convolution of THG signals can be quite complicated in anisotropic crystals and with a fundamental beam which is multimode. Particularly, we were mindful of the fact that beam profiles change in a lens wave guide if the beam is not an eigenmode such as Hermite Gaussians.[28] Because our fundamental beam was not filtered to make it single mode and because the precise nature of the multimode structure was not known, we adopted an empirical deconvolution procedure.

First, the focusing distance was adjusted to give optimum fringe contrast for a 2° BK-7 glass wedge. This was, in principle, a compromise between reduced beam waist, depth of focus, and changing beam profile. Next, since the theoretical plane wave or near-field fringe patterns are simply superpositions of sine waves, some simple convoluting profiles $g(x)$ were used in

$$\begin{aligned} S(x)&=\int g(x'-x)\sin^2(2\beta x')dx' \\ &=\int g(x'-x)\tfrac{1}{2}[1-\cos(\beta x')]dx' \ . \end{aligned} \tag{B1}$$

Some simple closed-form results for different profiles are as follows.

Rectangle:

$$S(x)=\tfrac{1}{2}[1-\mathrm{sinc}(\beta a)\cos(\beta x)] \ . \tag{B2}$$

Cosine:

$$S(x)=\tfrac{1}{2}\{1-\cos(\beta a)\times[1-(2\beta a/\pi)^2]^{-1}\cos(\beta x)\}\ . \quad \text{(B3)}$$

Circle:

$$S(x)=\tfrac{1}{2}\{1-J_1(\beta a)[\beta a/2]^{-1}\cos(\beta x)\}\ . \quad \text{(B4)}$$

Hollow circle:

$$S(x)=\tfrac{1}{2}\{1-[(a-c)\beta/2]^{-1}\times[J_1(\beta a)-J_1(\beta c)]\cos(\beta x)\}\ . \quad \text{(B5)}$$

Here a is the half-width for the first two profiles and is the larger radius for the second two; c is the inner radius for the last. $J_1(x)$ is a Bessel function of the first kind.

While all of these model profiles give drastically different magnitudes of the fringe contrast for fixed βa, the agreement of relative ratios as β is scaled are remarkably constant. Therefore, we ran a number of wedges with different wedge angles and of different *isotropic* materials including a very small angle wedge which gave a near unity contrast ratio which shows that beam profile changes are unimportant as the model requires. The simple fringe patterns were fit by the computer and the contrast ratios were found to follow this "universal" curve. The data reported in this work were also scaled by this same curve.

[1]J. P. Coffinet and F. de Martini, Phys. Rev. Lett. 22, 60 (1969).

[2]E. Yablonovitch, C. Flytzanis, and N. Bloembergen, Phys. Rev. Lett. 29, 865 (1972).

[3]S. D. Kramer, F. G. Parsons, and N. Bloembergen, Phys. Rev. B 9, 1853 (1974); S. D. Kramer and N. Bloembergen, *ibid.* 14, 4654 (1976).

[4]C. Flytzanis, in *Quantum Electronics,* edited by H. Rabin and C. L. Tang (Academic, New York, 1975), Vol. I, Part A, p. 9.

[5]C. Flytzanis and N. Bloembergen, Prog. Quantum Electron. 4, 271 (1976).

[6]See, for instance, S. K. Kurtz, in *Quantum Electronics,* edited by H. Rabin and C. L. Tang (Academic, New York, 1975), Vol. I, Part A, p. 209.

[7]G. R. Meredith (unpublished).

[8]See, for instance, N. Bloembergen, *Nonlinear Optics* (Benjamin, New York, 1965).

[9]We have borrowed heavily from B. F. Levine and C. G. Bethea, J. Chem. Phys. 63, 2666 (1975).

[10]We correct here the comment of Flytzanis and Bloembergen in Ref. 5, p. 274. Polarization is doubly modulated and intensity is triply modulated.

[11]P. N. Butcher, *Nonlinear Optical Phenomena* (Ohio State University Engineering, Columbus, 1965).

[12]J. F. Ward and G. H. C. New, Phys. Rev. 185, 57 (1969).

[13]It is straightforward to show that a circle results without the interface transmission corrections. These corrections are a fixed proportion of the field strength, which is the distance from the $\xi=-\infty$ point. The corrections then correspond to a uniform dilation or contraction of the two-space, preserving the circle. A small free-wave contribution should also be generated at each interface due to the discontinuous bound waves. Pictorially, a fixed-length line segment tangent to the vibration diagram subsequent to transmission correction is added. The circle is preserved since the template which rotates around the circle is still a fixed shape. We have not included this aspect in the diagrams to avoid further complexity and since it is a minor effect.

[14]G. R. Meredith, Rev. Sci. Instrum. (in press).

[15]M. Laikin, J. Opt. Soc. Am. 51, 238 (1961); *American Institute of Physics Handbook,* 2nd ed., edited by D. E. Gray (McGraw-Hill, New York, 1963), pp. 6–24.

[16]M. M. Choy and R. L. Byer, Phys. Rev. B 14, 1693 (1976).

[17]J. Jerphagnon, Appl. Phys. Lett. 16, 298 (1970).

[18]J. Jerphagnon and S. K. Kurtz, Phys. Rev. B 1, 1739 (1970).

[19]J. P. Hermann, Opt. Commun. 9, 74 (1973).

[20]P. D. Maker and R. W. Terhune, Phys. Rev. 137, A801 (1965).

[21]R. W. Hellwarth, Prog. Quantum Electron. 5, 1 (1977).

[22]T. Yajima, J. Phys. Soc. Jpn. 21, 1583 (1966).

[23]J. J. Gagnepain and R. Besson, Phys. Acoust. Princ. Meth. 11, 245 (1975).

[24]B. F. Levine, Phys. Rev. Lett. 22, 787 (1969).

[25]B. F. Levine, Phys. Rev. Lett. 25, 440 (1970).

[26]D. Bedeaux and N. Bloembergen, Physica (Utrecht) 69, 57 (1973).

[27]J. Ducuing, in *Nonlinear Optics,* edited by P. G. Harper and B. S. Wherrett (Academic, New York, 1977), p. 11.

[28]See, for instance, D. Marcuse, *Light Transmission Optics* (Van Nostrand Reinhold, New York, 1972).